VALIDATION OF PRECIPITABLE WATER ESTIMATED BY USING COST-EFFECTIVE GNSS RECEIVER SYSTEM

Taiki Takeda[1], Keiji Imaoka[1], Hidenori Shingin[1], and Kakuji Ogawara[1]

[1]Yamaguchi University, 2-16-1 Tokiwadai, Ube, Yamaguchi 755-8611, Japan

Email: b048vdv@yamaguchi-u.ac.jp

KEY WORDS: GNSS, low-cost receiver, precipitable water, multi-GNSS, PPP

ABSTRACT: In recent years, the Global Navigation Satellite System (GNSS) is indispensable in the field of position measurement. Although GNSS is widely used for positioning, it is also used as a means of measuring water vapor by utilizing the propagation delay of GNSS signals due to water vapor in the air. Although water vapor estimates from a GNSS continuous observation system GEONET, which is operated by the Geospatial Information Authority of Japan, are already being used for numerical weather forecasting in the Japan Meteorological Agency (JMA), increasing the station density will benefit further improvement of the forecasting. The use of dual-frequency low-cost GNSS receiver and antenna (cost-effective system) has the potential to solve both the density and associated cost issue. Although there are several investigations confirmed the performance of low-cost receivers in the zenith total delay (ZTD) estimation, direct comparison with in-situ data to verify the precipitable water (PW) estimates, which is the vertically integrated water vapor amount, has not been reported. In this research, a cost-effective system (u-blox ZED-F9P receiver with QZG12fQ antenna of Komine Musen Denki Co., LTD) was installed at the Matsue Local Meteorological Office MLMO of JMA, where operational radiosonde observations are performed. PW estimates by the cost-effective system was validated by using collocated PW values from the radiosonde and nearby GEONET observations. The validation results for the cost-effective system under the GPS-only processing showed less accurate performance in bias-removed root-mean-square-error, compared to those by GEONET under the same reception condition. By adding the GLONASS satellite in the processing, the performance significantly improved, probably because that the sufficient number of satellites became available by adding GLONASS satellites. Although the bias error needs to be further examined, the cost-effective system exhibited very promising capability in estimating PW.

1. INTRODUCTION

In recent years, extreme weather events such as record heavy rains and sudden downpours have been increasing in Japan. In order to prepare for the flood damages caused by such events, it is necessary to acquire water vapor information quickly and accurately. The Global Navigation Satellite System (GNSS) is generally used to acquire position information, but it is also used as a means of water vapor measurement using the propagation delay of GNSS signals. The Geospatial Information Authority of Japan (GSI) is operating a GNSS continuous observation system GEONET consisting of more than 1,300 stations with about 20 km spatial interval. Although water vapor estimates from GEONET data are already being used for numerical weather forecasting in the Japan Meteorological Agency (JMA), increasing the station density will benefit further improvement of the forecasting. One of the bottlenecks toward the high-density network is the cost issue of geodetic-grade receiver system. Therefore, the use of dual-frequency low-cost GNSS receiver and antenna (cost-effective system) will improve this situation. In addition, with the spread of connected cars in recent years, high-density dynamic observation network could be constructed by mounting cost-effective systems. In order to realize this, it is indispensable that the low-cost receiver has the same level of accuracy for water vapor estimation as the geodetic-grade receiver like one used in GEONET. Although there are several investigations confirmed the performance of low-cost receivers in the zenith total delay (ZTD) level, direct comparison with in-situ data to verify the water vapor estimates has not been reported. In this research, a cost-effective system was actually installed and operated adjacent to operational radiosonde observations, and direct validation of estimated precipitable water (vertically integrated amount of water vapor, PW) was performed. We also performed the comparison with precipitable water estimates from nearby GEONET station data, assessed the advantages of multi-GNSS utilization, and discussed the results.

2. METHOD

2.1. Experimental Setup

In this subsection we describe the cost-effective system used in the experiment. The cost-effective system consists of ZED-F9P of u-blox (Figure 1c) and QZG12fQ of Komine Musen Denki Co., LTD (Figure 1d). ZED-F9P is a dual-frequency low-cost receiver which can receive both L1 and L2 signals of most of the satellite systems. Combination of dual-frequency signals to eliminate the ionospheric effect is essential for the Precise Point Positioning (PPP) which is necessary for precipitable water estimation. However, ZED-F9P can only receive the latest L2C signals, which are not available for older generation GPS satellite like Block IIR. QZG12fQ is a dual-frequency high-precision antenna with reasonable cost. Data logging is performed using "rtkrcv" command-line application of RTKLIB (Takasu, 2022) program package (version 2.4.3 b34) installed on Raspberry Pi 3. The reception interval of the receiver is set to 30 seconds. Obtained data are automatically sent to the remote server via 3G network once a day. The cost-effective system was installed at the Matsue Local Meteorological Office (MLMO) of JMA, Shimane Prefecture, Japan, where operational radiosonde observations are performed by the Automatic Balloon Launcher (ABL) twice a day at 0900 and 2100 Japan Standard Time (JST). The installation environment at MLMO is almost clean, except the partial blockage of view in north-west direction by meteorological observation tower as seen in Figures 1a and 1b. To compare with the data from the cost-effective system, data obtained by nearby GEONET station named "MATSUE" with station number of 0074 were used. The station is located approximately 2.8 km apart from MLMO. The station utilizes the geodetic-grade system with TOPCON NETG5 as a receiver and TPSCR.G5 GSI as antenna. Data in RINEX format are available from GSI website. In this paper, we used the data obtained by the cost-effective system, GEONET station, and radiosonde observations during from December 18 in 2021 to August 13 in 2022. From February 26 to April 25, the radiosonde observation was suspended due to the facility maintenance.

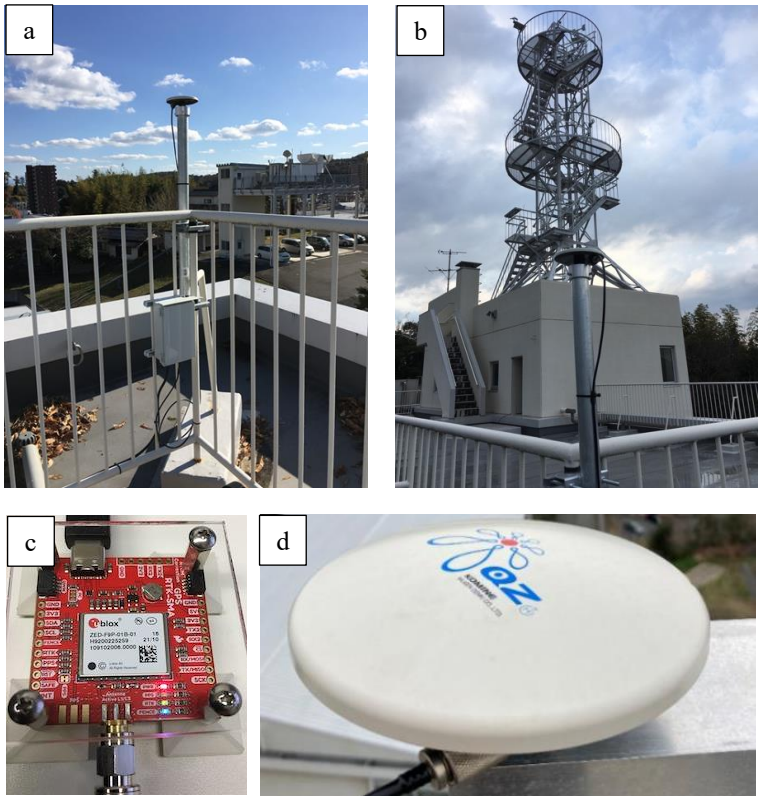

Figure 1. Experiment setup of cost-effective system at MLMO building. (a) Overall view of experiment setup from north-west direction (ABL is seen behind the cost-effective system), (b) same from south-east direction (observation tower is seen behind the antenna), (c) ZED-F9P, and (d) QZG12fQ.

2.2. Post-processing and ZTD estimation

After the conversion of raw log files into RINEX formatted data, we used "rnx2rtkp" command-line application of RTKLIB for post-processing and calcuration of ZTD values. Major specifications of the post-processing is summarized in Table 1. We used PPP-static as the analysis method. Unlike the RTK method, it performs positioning with only one receiver without using nearby base station data. Assuming that the accurate-enough information including precise orbit and clock solutions of the satellites, ionospheric correction by dual-frequency signals, and the corrections for phase center variation (PCV) of satellite/station antennas are given, it is possible to perform positioning at an accuracy of seveal millimeters without using double phase difference. In this study, we used the orbit/clock final solutions provided by the Internatinal GNSS Service (IGS) for the GPS analysis. In addition, orbit/clock final solutions provided by the Center for Orbit Determination in Europe (CODE) within the framework of Multi-GNSS Experiment (MGEX) of IGS, was used for multi-GNSS analysis. The final solution is the refined product with the highest quality that appears two weeks after the data is acquired. For the PCV correction, "ngs14.atx" calculated by the National Geodetic Survey (NGS) was used for the satellites and cost-effective system, and "GSI_PCV.pcv" calculated by GSI was used for GEONET system. For the correction of tidal loading, we used the calculation results by the ocean tidal loading provider (with NAO.99b model), maintained by the Chalmers University of Technology. For the post-processing, we input two-days RINEX data in one process, and extracted the second half to obtain the solution. The reason is that the PPP-static anaysis with forward Kalman filtering seems to need several hours to be stabilized. The following five combinations were used to calculate ZTD values; cost-effective system plus GPS (with L2C), cost-effective system plus multi-GNSS (GPS+GLONASS), GEONET plus GPS (with L2C), GEONET plus all GPS, and GEONET plus multi-GNSS (GPS+GLONASS). Because of the limition of receivable L2 signal by the cost-effective system, the third combination was used to evaluate the performance under the same condition between cost-effective and GEONET systems.

Table 1. Major specifications of post-processing

Positioning method	PPP-static
Elevation cutoff	10 degree
Clock & orbit solution (GPS)	IGS Final
Clock & orbit solution (GPS+GLONASS)	CODE Final
Analysis interval	30 seconds
Antenna PCV correction (satellite and cost-effective)	ngs14.atx
Antenna PCV correction (GEONET)	GSI_PCV.pcv

2.3. PW calculation from ZTD

This subsection describes the method of converting ZTD obtained by RTKLIB "rnx2rtkp" to PW. The zenith hydrostatic delay (ZHD), which is the delay due to dry air calculated from the surface pressure, is subtracted from ZTD to calculate the zenith wet delay (ZWD), which is the delay due to water vapor (Arief and Heki, 2020). The surface pressure P in hPa was calculated by an approximated form of barometric formula as

$$P = P_{msl} \times \left(1 - \frac{0.0065 \times h}{T_s - 0.0065 \times h + 273.15}\right)^{5.257}, \quad (1)$$

Where h is the geodetic altitude in meters, T_s is the surface air temperature in kelvin, and P_{msl} is the sea level pressure. The surface air temperature and sea level pressure were derived from the surface meteorological observations at MLMO. ZHD was computed by (Davis, 1985)

$$\mathrm{ZHD} = (0.0022768) \times \frac{P}{1 - 0.00266cos2\varphi - 0.00000028h}\,, \tag{2}$$

where φ is the observation station latitude. Then, ZWD was obtained by

$$\mathrm{ZWD} = \mathrm{ZTD} - \mathrm{ZHD}. \tag{3}$$

ZWD obtained by Equation (3) and PW have the relationship (Askne and Nordius, 1987) expressed by

$$\mathrm{PW} = \frac{10^5}{R_v\left(k_2 - k_1\frac{m_v}{m_d} + \frac{k_3}{T_m}\right)} \cdot ZWD, \tag{4}$$

where $k_1 = 77.60$ [K/hPa], $k_2 = 71.98$ [K/hPa], $k_3 = 3.754 \times 10^5$ [K/hPa], the specific gas constant of water vapor $R_v = 461$ [J/kg · K], the molecular weight of water vapor $m_v = 18.0152$ [kg/kmol], the molecular weight of dry air $m_d = 28.9644$ [kg/kmol], and T_m is the weighted average temperature in kelvin representing the average temperature weighted by the water vapor partial pressure above the observation point. The values of constants k_1, k_2, and k_3 were based on the previous research (Boudouris, 1963). From two years of radiosonde observations in North America, the relationship between T_m and T_s was found (Bevis, 1992) as

$$T_m \approx 70.2 + 0.72T_s. \tag{5}$$

2.4. PW calculation from radiosonde profile

In this subsection we describe how to calculate PW from radiosonde observations (Nishimura, 2002). The saturated water vapor pressure e_s in hPa was calculated from the air temperature for each observation level by

$$\ln\left({}^{e_s}/_{6.11}\right) = {}^{\mathrm{L}\left({}^{1}/_{273} - {}^{1}/_{T}\right)}\Big/_{R_v}, \tag{6}$$

where T is the air temperature in kelvin and $\mathrm{L} = 2.50 \times 10^6$ [J/kg] is the latent heat. From the obtained e_s and relative humidity, the water vapor pressure e in hPa at each observation level was obtained by

$$\mathrm{e} = e_s \cdot RH/100\,, \tag{7}$$

where RH is relative humidity in percentage. The mixing ratio W in g/kg for each observation level was obtained by

$$\mathrm{W} = \varepsilon \cdot e/(P - e)\,, \tag{8}$$

where $\varepsilon = m_v/m_d = 0.622$ and P is the atmospheric pressure at the level in hPa. The PW value of the radiosonde observation PW_{sonde} in millimeters can be derived by integrating the obtained mixing ratio with atmospheric pressure by

$$PW_{sonde} = \frac{1}{g}\int_{Ps}^{p_{top}} W dp\,, \tag{9}$$

and practically computed by

$$PW_{sonde} = \sum\left\{\frac{(W_i + W_{i+1})}{2g}\right\}(P_i - P_{i+1}) \times 10^3\,, \tag{10}$$

where P_{top} is the pressure at the top of the atmosphere in hPa, P_s is the pressure at the radiosonde launch point in hPa, P_i is the pressure at the i[th] observation level in hPa, W_i is the mixing ratio at the i[th] observation level in g/kg, W_{i+1} is the mixing ratio at the (i+1) [th] observation level in g/kg, $and\ g = 9.8\ [m/s^2]$ is the gravitational acceleration.

3. RESULT AND DISCUSSION

Time-serie variations of PW values obtained by GNSS and radiosonde observations were shown in Figure 2. During the data gap of radiosondes, all the plots were not drawn. The period of observation covered the seasons from winter to summer, resulted in the PW range around from 5 to 65 mm, which almost covered the typical dynamic range of PW value in Japan. The performance of GNSS PW was evaluated in comparison with rasiosonde observations by using root-mean-square error (RMSE), bias error, and the RMSE after removed the bias error. The values are summarized in Table 2 for five cases and corresponding scatter plots are shown in Figure 3. In case of using GPS satellites with L2C signal, the cost-effective system indicated larger errors in all aspects compared to those by GEONET. In this case, GEONET system showed almost no bias error and 1.27 mm of RMSE. As seen in Figure 3, the scatter plots for the cost-effective system apparently showed larger scatters. By adding all available GPS satellite (i.e., Block IIR satellites which are not receivable by cost-effective system) to GEONET processing, the performance was further improved. In case of using GPS and GLONASS satellites in the processing, the RMSE value for the cost-effective system reduced to 1.84 mm, although the bias error remained the same. The RMSE (bias-removed) value significantly improved to 1.27 mm, which was almost the same as the result by GEONET system in case of using GPS with L2C. For the GEONET system, this satellite combination provided better RMSE (bias-removed), but introduced the bias error of -0.41 mm. In summary, except for the bias error of -1.33 mm, the cost-effective system indicated comparable performance to that by GEONET system in terms of variability, under the multi-GNSS condition.

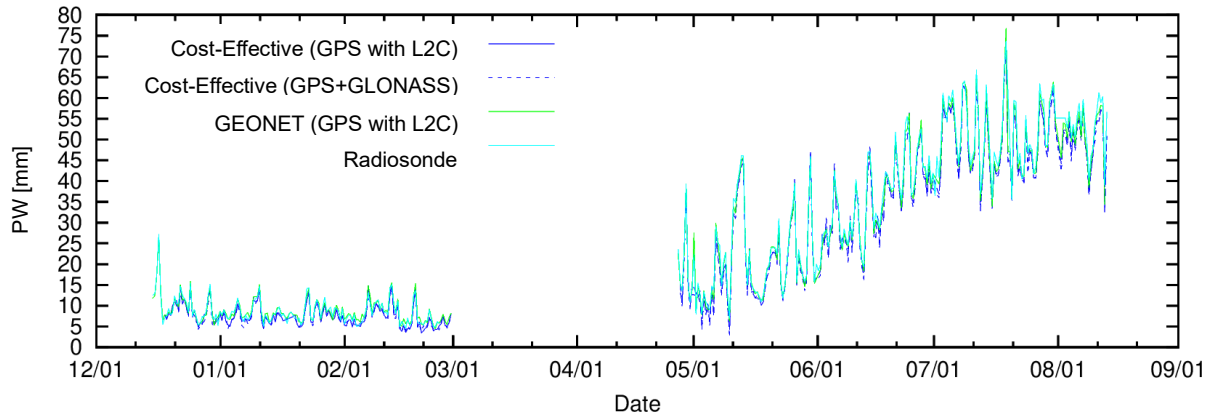

Figure 2. Time-series variation of PW from each receiver and radiosonde.

Table2. PW comparison with radiosonde

	RMSE [mm]	Bias [mm]	RMSE (bias-removed) [mm]
Cost-Effective (GPS with L2C)	2.19	-1.33	1.74
Cost-Effective (GPS+GLONASS)	1.84	-1.33	1.27
GEONET (GPS with L2C)	1.27	-0.01	1.27
GEONET (GPS ALL)	1.18	-0.02	1.18
GEONET (GPS+GLONASS)	1.26	-0.41	1.19

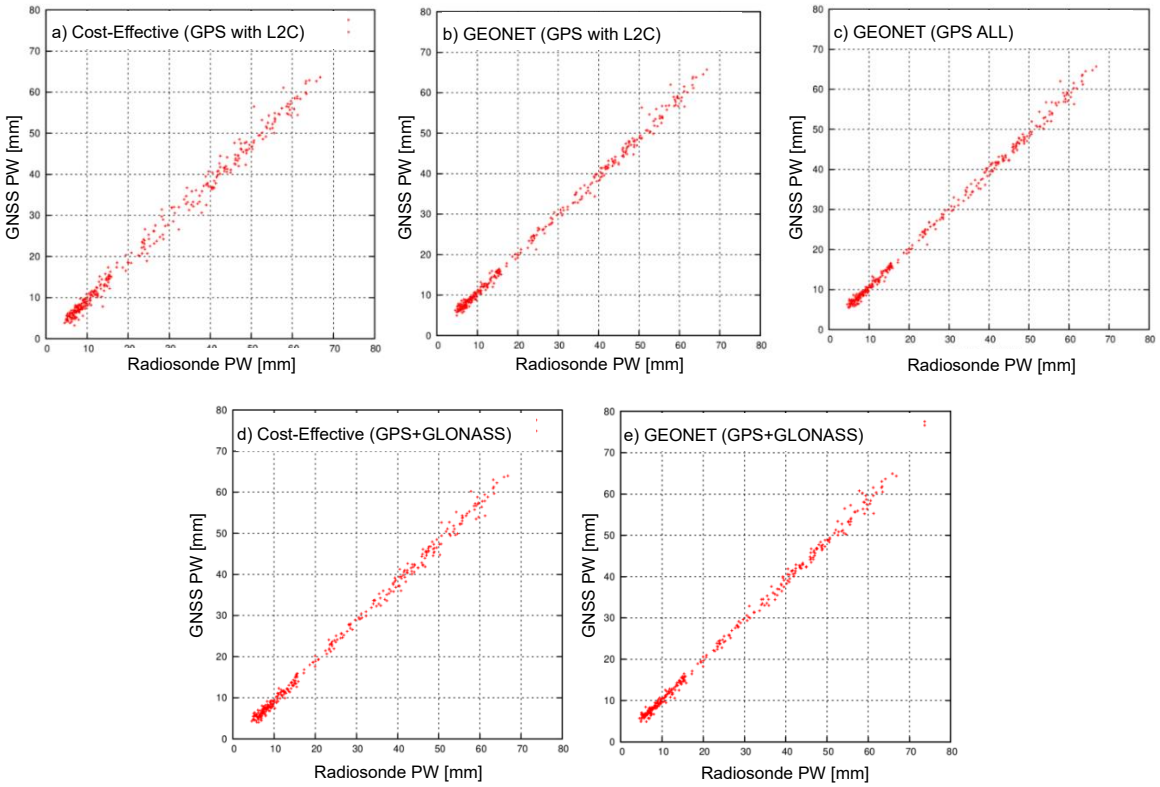

Figure 3. PW scatterplots by different system and satellite combinations. a) Cost-Effective system (GPS with L2C), b) GEONET (GPS with L2C), c) GEONET (GPS ALL), d) Cost-Effective (GPS+GLONASS), and e) GEONET (GPS+GLONASS).

One of the potential reasons for the difference in performance between the cost-effective system and GEONET in case of using GPS satellites with L2C signal is that the observation tower located in north-west direction of the cost-effective system became an obstacle and reduced the number of visible satellites. Figure 4 shows the satellite position at 2100 JST on June 14, 2022 for the L1 frequency. In the vicinity of the satellite marked with a circle on the right side panel for the cost-effective system, we can see that the reception condition became worse and produced many cycle-slips. This poor reception area in the north-west direction coincided with the direction of the observation tower. For the PW estimates of the cost-effective receiver by using GPS satellites with L2C signal, in which the number of available satellites is intrinsically small, further reduction of the number of satellites due to obstacles may degrade the performance. By adding the GLONASS satellites, the number of satellites might reach to the enough level and the effect due to the above-mentioned obstacles was almost canceled out. In the near future, with the increase of new generation of GPS satellites, this issue will be resolved even for the GPS-only analysis. In Figures 3 and 5, we can observe that the variability increased with PW value particularly for the cost-effective system with GPS. In the multi-GNSS analisys for the cost-effective system, the variability was largely reduced particularly at high PW values. Although we need to further confirm, it is possible that the increase of the available satellites may be more effective in the high PW range, where the spatial inhomogeneity of PW may be more significant.

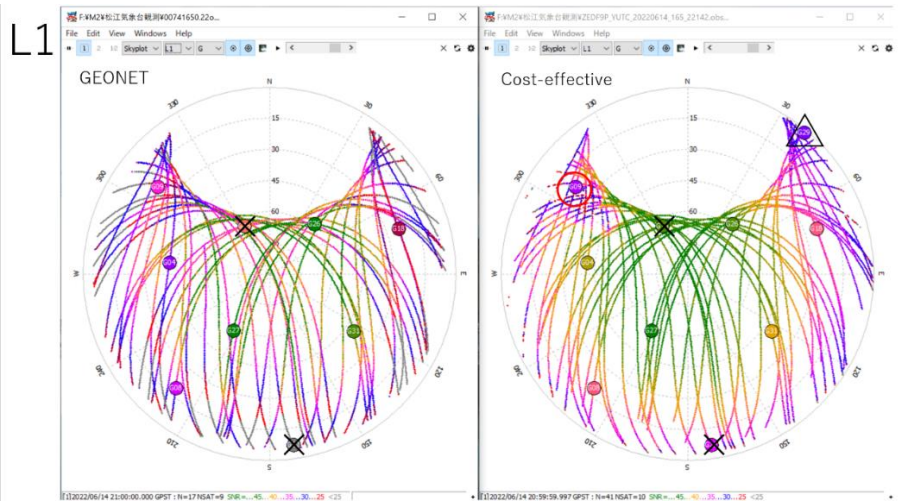

Figure 4. Satellite positions at 2100 JST on June 14, 2022 in L1 frequency for GEONET (left) and cost-effective system (right). Cross marks indicate the satellites without L2C signal, and triangle marks show the excluded satellites due to elevation mask.

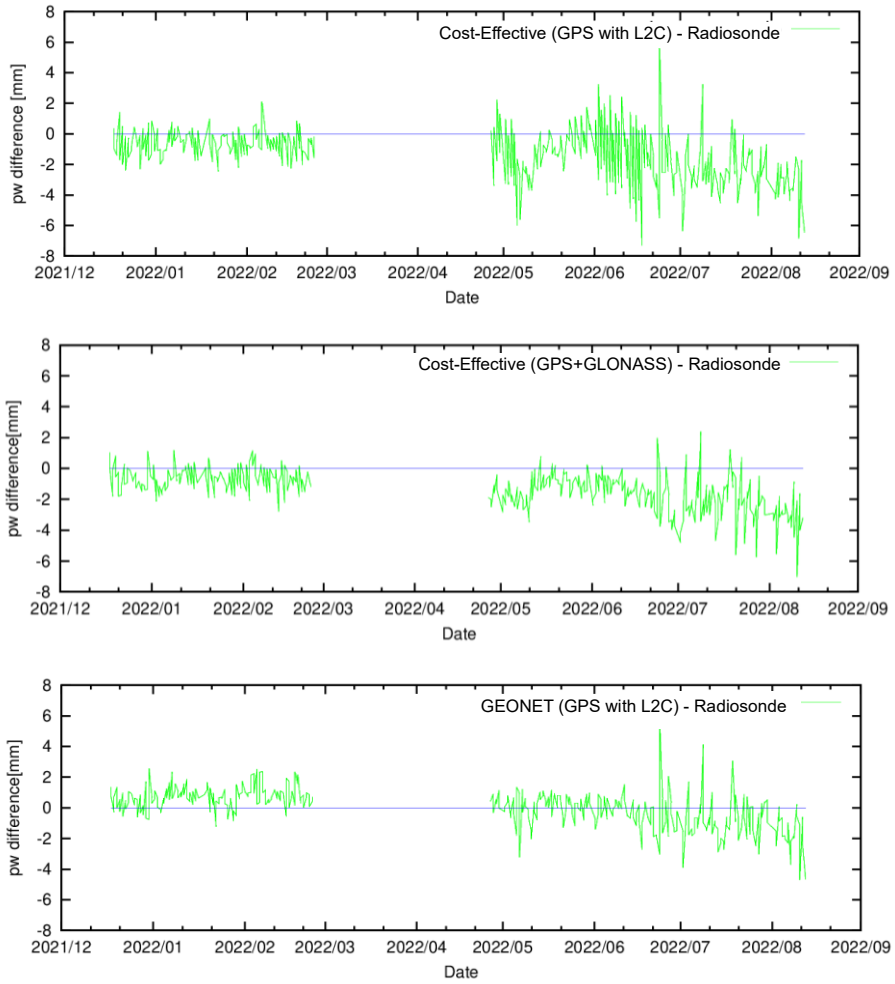

Figure 5. Time series of PW difference (GNSS minus radiosonde). From top to bottom, Cost-Effectivae system (GPS with L2C), Cost-Effective system (GPS+GLONASS), and GEONET (GPS with L2C).

4. CONCLUSION AND FUTURE

In this study, a cost-effective GNSS system was installed in the vicinity of operational radiosonde observation at MLMO of JMA, and the PW estimation accuracy by the cost-effective receiver was directly verified by comparing with those from radiosonde observations and nearby GEONET station. With the cost-effective system under the GPS-only processing, PW estimates showed larger errors compared to those by GEONET. The possible reason was that, in addition to the intrinsically small number of available satellites which limited to the ones with L2C signal capability, visible satellites had further decreased due to the partial sky blockage by the MLMO observation tower. Under the multi-GNSS condition utilizing GPS and GLONASS satellites, although there was persistent bias error of -1.33 mm, the cost-effective system was able to produce PW estimates with mostly comparable performance compared to GEONET, with the RMSE (bias-removed) of 1.27 mm, which was almost consistent with the one by GEONET under the GPS-only processing. Although we further need to investigate the reason of the bias error, we were convinced that the performance of the cost-effective system in estimating PW values is very promising. Our ultimate goal is to assess the possibility of high-density dynamic observation network of PW by mounting the cost-effective system on moving vehicles. Under such conditions, a system is constantly moving, and the condition of the field of view rapidly changes. Similar to the result in this paper, multi-GNSS capability may be very effective in establishing stable reception condition and lead to better PW estimates.

REFERENCES

Arief, S., and K. Heki, 2020. GNSS meteorology for disastrous rainfalls in 2017-2019 summer in SW Japan: A new approach utilizing atmospheric delay gradients. Front. Earth Sci., 8. doi: 10.3389/feart.2020.00182

Askne, J. and H. Nordius, 1987. Estimation of tropospheric delay for microwave from surface weather data. Radio Sci., 22 (3), pp. 379-386.

Bevis, M., S. Businger, T. A. Herring, C. Rocken, R. A. Anthes, and R. H. Ware, 1992. Remote sensing of atmospheric water vapor using the Global Positioning System. J. Geophys. Res. Atmos., 97, pp. 15787–15801.

Boudouris, G., 1963. On the index of refraction of air, the absorption and dispersion of centimeter waves by gasses. J. Res. Natl. Bur. Stand., 67D (6), pp. 631-684.

Davis, J. L., T. A. Herring, I. I. Shapiro, A. E. E. Rogers, and G. Elgered, 1985. Geodesy by radio interferometry: Effects of atmospheric modeling errors on estimates of baseline length. Radio Sci., 20 (6), pp. 1593-1607.

Nishimura, M., 2002. A comparison of precipitable water vapor obtained from GPS and radiosonde. Geosci. Repts. Shizuoka Univ., 29, pp. 61-75.

Takasu, T., 2022. RTKLIB: An Open Source Program Package for GNSS Positioning. Retrieved September 19, 2022, from https://www.rtklib.com/.

ACKNOWLEDGMENT

Authors are extremely grateful to JMA colleagues, particularly Mr. Ken Kinutani and Mr. Hidenori Hatta, for their intensive support in the installation and operation of the cost-effective system at MLMO.The GEONET data and their antenna calibration data were provided by GSI. Precise satellite orbit/clock solutions and antenna calibration data for satellites/cost-effective antenna were provided by IGS and NGS, respectively. Radiosonde profiles were extracted from JMA website. This work was supported by JSPS KAKENHI Grant Number JP20K21847.